Dynamics of liquid films exposed to high-frequency surface vibration

Ofer Manor*
Wolfson Department of Chemical Engineering, Technion—Israel Institute of Technology, Haifa 32000, Israel

Amgad R. Rezk, James R. Friend, and Leslie Y. Yeo†
Micro/Nanophysics Research Laboratory, RMIT University, Melbourne, VIC 3001, Australia

(Received 11 February 2015; published 19 May 2015)

We derive a generalized equation that governs the spreading of liquid films under high-frequency (MHz-order) substrate vibration in the form of propagating surface waves and show that this single relationship is universally sufficient to collectively describe the rich and diverse dynamic phenomena recently observed for the transport of oil films under such substrate excitation, in particular, Rayleigh surface acoustic waves. In contrast to low-frequency (Hz- to kHz-order) vibration-induced wetting phenomena, film spreading at such high frequencies arises from convective drift generated by the viscous periodic flow localized in a region characterized by the viscous penetration depth $\beta^{-1} \equiv (2\mu/\rho\omega)^{1/2}$ adjacent to the substrate that is invoked directly by its vibration; μ and ρ are the viscosity and the density of the liquid, respectively, and ω is the excitation frequency. This convective drift is responsible for driving the spreading of thin films of thickness $h \ll k_l^{-1}$, which spread self-similarly as $t^{1/4}$ along the direction of the drift corresponding to the propagation direction of the surface wave, k_l being the wave number of the compressional acoustic wave that forms in the liquid due to leakage of the surface wave energy from the substrate into the liquid and t the time. Films of greater thicknesses $h \sim k_l^{-1} \gg \beta^{-1}$, in contrast, are observed to spread with constant velocity but in a direction that opposes the drift and surface wave propagation due to the attenuation of the acoustic wave in the liquid. The universal equation derived allows for the collective prediction of the spreading of these thin and thick films in opposing directions.

DOI: 10.1103/PhysRevE.91.053015 PACS number(s): 47.55.nd, 47.61.−k, 47.35.Rs

I. INTRODUCTION

High-frequency vibration in solids, assuming the form of acoustic waves with frequencies in a similar range to high-frequency (3–30 MHz) and very high frequency (30–300 MHz) radio electromagnetic waves, were recently found to be capable of driving novel drop and film wetting dynamics [1–8] distinct from that excited by their lower-frequency counterparts [9–19]. In low-frequency studies, usually at frequencies comparable to the natural oscillation frequency of the liquid body (∼10 Hz–10 kHz), the liquid generally responds through the generation of a predominantly convective (potential) flow in the bulk [20,21]. This leads to shape oscillations of the liquid body modulated by the restoring force imposed by its surface tension [22,23], manifesting as patterns on the free surface of liquid films [9–11,14,24]. In addition, these shape oscillations can cause displacement of the three-phase contact line in sessile drops that, in turn, results in a change in the contact angle beyond its hysteresis range, rendering periodic stick-slip contact line motion [18,25–27] and enabling drop translation [13,17,19].

Such vibrational excitation also invokes a viscous-dominant periodic vortical flow field in a thin region adjacent to the solid substrate with a thickness characterized by a viscous penetration length $\beta^{-1} \equiv (2\mu/\rho\omega)^{1/2}$, where μ and ρ denote the liquid viscosity and density, respectively, and ω the angular frequency of excitation. This periodic boundary layer flow, first examined by Stokes for simple in-plane periodic substrate motion (see, for example, Batchelor [28]), was subsequently extended by Schlichting (hence the flow being commonly referred to as Schlichting boundary layer flow or Schlichting streaming) and others to account for more complicated forms of excitation, where the substrate motion, or, alternatively, the bulk fluid motion, comprises a periodic standing wave with a wavelength smaller than the characteristic length scale of the substrate [29–41] and, recently, where the substrate motion comprises propagating, generalized surface waves (SWs) [42].

Much less is yet understood, however, concerning how high-frequency substrate vibration influences the dynamics of spreading films despite considerable interest of late in such systems given their utility for manipulating flow at microscale and nanoscale dimensions for a variety of microfluidic applications [43,44]. The distinct behavior observed in high-frequency vibrational excitation appears to arise primarily at high frequencies above 1 MHz and was first realized when sessile water drops atop slightly hydrophilic substrates were excited by 2-MHz *bulk* pistonlike vibration [4]. In particular, the momentum generated as a consequence of such high-frequency vibration, in the form of Reynolds stresses, within a 400-nm-thick layer in the water drop immediately adjacent to the substrate over which viscous penetration of the compressional acoustic waves in the liquid occurs, was sufficient to cause the apparent contact angle of the drop to decrease. More specifically, the net force exerted at the air-water interface in the vicinity of the contact line was estimated to assume the form $F \sim 1/\beta^{-1} \sim \omega^{1/2}$, so the higher the applied frequency and thus the smaller the viscous penetration length, the greater the influence of the vibration on the dynamic change in the contact angle and thus the spreading of the liquid. It will be seen below that a similar inverse dependence of liquid spreading on the viscous penetration

*manoro@technion.ac.il
†leslie.yeo@rmit.edu.au

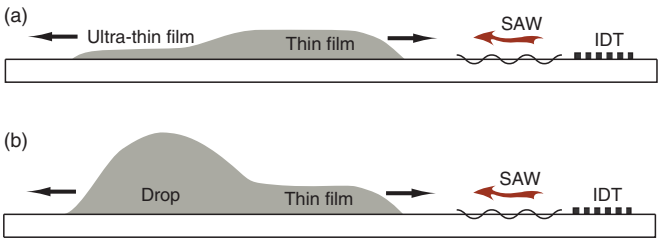

FIG. 1. (Color online) Schematic illustration of the spreading observed for liquids on high-surface-energy substrates vibrating at high frequencies under Rayleigh surface acoustic wave (SAW) excitation generated by interdigitated transducer (IDT) electrodes deposited on a piezoelectric substrate. (a) Thin submicron films spread along the propagation direction of the SAW, whereas films of intermediate thicknesses spread in the other direction, opposing that of the SAW propagation. (b) Sessile drops (or thick submillimeter films), on the other hand, advance along the SAW propagation direction.

length associated with the substrate vibration is consistently observed in other high-vibration-frequency systems.

Similar characteristics are observed, for example, in the spreading of thin films of low-surface-tension, i.e., highly wetting liquids, such as silicone oils under the excitation of high-frequency Rayleigh surface acoustic waves (SAWs). Unlike the high-surface-tension water drops that, given their finite contact angle, possess millimeter-order thicknesses comparable to the capillary length scale—large with respect to β^{-1} under such high-frequency vibration, low-surface-tension films typically possess thicknesses comparable to β^{-1}, giving rise to distinct spreading dynamics. In these cases, the viscous-dominant periodic flow field, associated with the viscous penetration of the vibration into the liquid, no longer behaves as boundary layer flows [39] in the strictest sense. In contrast, these sufficiently thin films possess flow fields that are bounded by their free surface such that their dynamics are increasingly governed by convective processes, thus taking the form of inertial films [45,46], as will be seen subsequently. Additionally, these oil films also exhibit a thickness-dependent double spreading reversal phenomenon. Thin submicron films that initially spread *along* the propagation direction of the SAW were observed to reverse their direction above a critical film thickness such that films of intermediate thickness, typically several microns to tens of microns in height, spread in the direction *opposing* that of the SAW propagation [Fig. 1(a)]. Increasing the film thickness further beyond a second critical value, however, triggered a second spreading reversal wherein thick submillimeter films and sessile drops were observed to translate again *along* the SAW propagation direction [Fig. 1(b)] [8].

In this paper we derive a unified theory that describes the dynamic spreading behavior of liquid films atop high surface energy substrates excited by high-frequency vibration in the form of generalized traveling SWs, which include, but are not necessarily limited to, Rayleigh SAWs. We begin in Sec. II by formulating the equations governing the conservation of mass and momentum subject to the relevant boundary conditions for the vibrating substrate and the free surface of the film that are then used to derive a generalized film spreading equation that describes the spatiotemporal evolution of the film. This is then simplified in Sec. III to first analyze thin films whose thickness h is considerably smaller than the wavelength $2\pi/k_l$ of the compressional acoustic waves that form in the liquid due to leakage of the surface wave energy from the substrate into the liquid. Here we will show that the spreading dynamics of these thin films, at least at thicknesses comparable to $h \approx \beta^{-1} \approx 10^2$–$10^3$ nm ($\ll 2\pi/k_l$)—away from the nanometer length scales where capillary and intermolecular forces are dominant—are determined by a balance between capillary forces and the convective drift that arises due to the SW excitation. Subsequently, we examine in Sec. IV thicker films that are comparable in thickness to the compressional acoustic waves in the liquid, $h \sim \mathcal{O}(2\pi/k_l)$, where the acoustic radiation pressure becomes appreciable, and investigate the film stability, wherein we observe that the thin films which are stable at sufficiently small thicknesses become periodically unstable at larger thicknesses. At these larger thicknesses, stable films, experiencing both convective drift and acoustic radiation pressure are observed to spread in a direction that opposes the drift and hence the SW propagation direction for the case in which the SW comprises a retrograde elliptical surface motion, such as the Rayleigh SAWs employed in our earlier experiments. As the films grow further in thickness, such that $h \gg 2\pi/k_l$, their spreading dynamics is dominated by a different mechanism which is not accounted for in our generalized film equation, that is, the Eckart streaming, which was previously considered elsewhere [8].

Finally, concluding remarks are provided in Sec. V, where we summarize the underlying physics that govern high-frequency acoustic film spreading.

II. GENERALIZED FILM SPREADING EQUATION

We consider a two-dimensional liquid film of thickness $h^*(x^*,t^*)$ that spreads atop a horizontal solid substrate. The coordinates x^* and y^* are measured along and transverse (normal) to the solid-liquid boundary, respectively, and t^* denotes time; henceforth, the asterisks (*) denotes dimensional quantities. As illustrated in Fig. 2, the substrate undulates due to vibration imposed in the form of a propagating harmonic SW, such as Lamb and flexural bulk waves, or Rayleigh and Sezawa SAWs [43], for example. The motion of the two-dimensional SW comprises both longitudinal and transverse surface velocities (along and normal to the substrate surface) with typically similar amplitudes χU^* and U^*, respectively, that differ in time by a phase difference φ. The SW, propagating along the x^* coordinate along the substrate surface $y^* = 0$, is

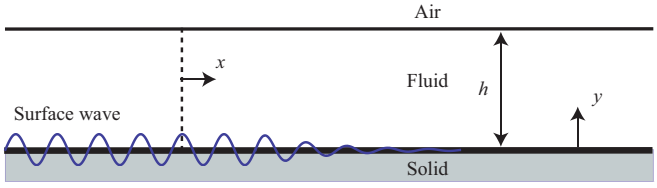

FIG. 2. (Color online) Schematic of the two-dimensional liquid film under excitation by surface waves propagating along the solid substrate.

further defined by a wave number k^*, an angular frequency ω^*, and an amplitude attenuation coefficient α^* and can be described in general form as follows:

$$\begin{pmatrix} u^*_{x^*} \\ u^*_{y^*} \end{pmatrix}_{\overline{x^*}} = \begin{pmatrix} \chi U^* e^{i(\omega^* t^* - k^* x^*) - \alpha^* x^*} \\ U^* e^{i(\omega^* t^* - k^* x^* + \varphi) - \alpha^* x^*} \end{pmatrix}; \tag{1}$$

the real part of which describes the actual physical SW and $\overline{x^*}$ determines the spatial coordinate of the solid surface that undergoes a corresponding motion transverse to, and along, the solid surface with respect to $(x^*, y^* = 0)$. While contributions from the motion of the solid surface may be appreciable under the influence of Hz- and kHz-order SWs, the amplitude of SWs in the MHz-order frequency regime that we examine are usually subnanometer to nanometer in magnitude—extremely small with respect to the thickness of the film—such that it is possible to neglect its contribution to the flow field and thus approximate $\overline{x^*} \approx (x^*, y^* = 0)$ to leading order.

The SW propagation at the solid-liquid boundary then gives rise to a predominantly viscous periodic flow, penetrating into the liquid over a distance characterized by the viscous penetration length $\beta^{*^{-1}}$ while supporting a weak convective drift that possesses a steady component. For $h^* \gg \beta^{*^{-1}}$, this flow attenuates in the bulk of the liquid and takes the form of a boundary layer flow [42]. On the other hand, it shall be seen that interactions between this flow, invoked by direct contact between the SW and the liquid, in the presence of the free surface associated with the film constitutes the primary mechanism for its spreading when $h^* \lesssim \beta^{*^{-1}}$. Further, energy from the SW leaks into the fluid at the Rayleigh angle $\theta_R = \sin^{-1} k^*/k_l^*$, measured from the positive y axis, resulting in the generation of longitudinal compressional acoustic waves (i.e., sound waves) in the liquid with wavelength λ_l^* and corresponding wave number k_l^* [43,47]. Should the film thickness be larger than or comparable to the acoustic wavelength in the liquid, i.e., $h^* \gtrsim k_l^{*^{-1}} \gg \beta^{*^{-1}}$, these acoustic waves impinge on the free surface, generating a net acoustic radiation pressure [43,48,49]. Additionally, attenuation of the acoustic waves propagating in the liquid renders an effective body force that invokes Eckart streaming [30,50,51].

In this section, we, however, first consider films where h^* scales as $\beta^{*^{-1}}$. The dominant flow in the film that arises, confined from below by the solid substrate along which the SWs propagate and from above by the free surface of the film, is governed by conservation equations similar to the classical boundary layer flow equations, noting that these have been used to model convective dynamics in thin films elsewhere [45,46,52]. We will therefore delay an extension of the analysis to film thicknesses that approach the acoustic wavelength in the liquid—usually large with respect to the viscous penetration length ($\beta^{*^{-1}} \ll k_l^{*^{-1}}$)— until Sec. IV.

For thin films with thicknesses on the order $\beta^{*^{-1}}$, the appropriate scaling for the variables associated with the flow field in the film are then

$$\begin{aligned} t^* \to \omega^{*^{-1}} t, \quad (x^*, y^*, h^*, \alpha^{*^{-1}}) \to k^{*^{-1}}(x, \eta y, \eta h, \alpha^{-1}), \\ (u_x^*, u_y^*) \to U^*(u_x, \eta u_y), \quad \psi^* \to k^{*^{-1}} \eta U^* \psi, \\ (p^*, p_r^*, \Pi^*) \to \eta k^* \gamma^* (p, p_r, \Pi), \quad \mathtt{A}^* \to \eta^4 k^{*^{-2}} \gamma^* \mathtt{A}, \end{aligned} \tag{2}$$

where $\eta \equiv \beta^{*^{-1}}/k^{*^{-1}}$ and ψ^* is a stream function satisfying $\mathbf{u}^* = (u_x^*, u_y^*) = (\partial_y \psi^*, -\partial_x \psi^*)$; γ^* is the interfacial tension, $\mathtt{A}^*$ is the Hamaker constant, and, p^*, p_r^*, and Π^* are the hydrodynamic pressure, acoustic radiation pressure, and disjoining pressure, respectively. The relevant boundary conditions are those that describe the SW motion on the substrate $y = 0$ given by Eq. (1) as well as that which embodies the tangential stress balance and normal stress jump at the free surface of the film $y = h(x,t)$ [8,46], i.e.,

$$\begin{pmatrix} u_x \\ u_y \end{pmatrix}_{y=0} = \begin{bmatrix} \chi e^{i(t-x)-\alpha x} \\ e^{i(t-x+\varphi)-\alpha x}/\eta \end{bmatrix} \tag{3}$$

and

$$\begin{pmatrix} \partial_y u_x \\ \partial_y u_y \end{pmatrix}_{y=h} = \begin{bmatrix} 0 \\ (\eta/2\mathtt{Ca})\,(p + 2\kappa + p_r - \Pi) \end{bmatrix}, \tag{4}$$

respectively, where $\kappa = \partial_{xx} h/2 + \mathcal{O}(\eta^2)$ is the mean curvature of the film and $\mathtt{Ca} \equiv \mu^* U^*/\gamma^*$ is the capillary number. Mass and momentum conservation further require [37,38]

$$\begin{aligned} \partial_y^4 \psi/2 = \epsilon\left[\partial_y \psi\, \partial_x\left(\partial_y^2 \psi\right) - \partial_x \psi\, \partial_y\left(\partial_y^2 \psi\right)\right] \\ + \partial_t\left(\partial_y^2 \psi\right) + \mathcal{O}(\eta^2), \end{aligned} \tag{5}$$

in which ω^*/k^* and $\epsilon \equiv U^* k^*/\omega^*$ represent the phase velocity and the Mach number of the SW propagating in the solid, respectively, and $(u_x, u_y) = (\partial_y \psi, -\partial_x \psi)$.

Two naturally small parameters, ϵ and η, are observed to appear in Eqs. (3) and (5). It is reasonable to require $\epsilon \ll \eta \ll 1$ given common values for the SW velocity amplitude $U^* \sim \mathcal{O}$ (0.01–1 m/s) under high-frequency excitation [42], in particular, $\omega^*/2\pi \approx 30$ MHz as a typical frequency of the Rayleigh SAWs used, for which $\varphi = 3\pi/2$. It then follows that $\omega^*/k^* \approx 4 \times 10^3$ m/s, $\chi \approx 1$, and $U^* \approx 0.1$ m/s, which, together with typical values characteristic of silicone oil used in the experiments, i.e., $\mu^* \approx 10^{-1}$ Pa s, $\rho^* \approx 10^3$ kg/m^3, and $\gamma^* \approx 10^{-2}$ N/m, give $\mathtt{Ca} \approx 1$, $\eta \approx 0.5 \times 10^{-1}$, $\epsilon/\eta \approx 0.5 \times 10^{-3}$, and $\epsilon \approx 2.5 \times 10^{-5}$.

We proceed by asymptotically expanding the flow variables using the following ansatz:

$$u_x = \sum_{n=-1}^{\infty} f_n u_{x,n}, \quad u_y = \sum_{n=-1}^{\infty} f_n u_{y,n}, \quad \psi = \sum_{n=-1}^{\infty} f_n \psi_n, \tag{6}$$

in which $f_{n+1} \ll f_n$ and in which $u_{x,n}$, $u_{y,n}$, and ψ_n are $\mathcal{O}(1)$. Although accounting for the formation of capillary waves in the following leading-order analysis, we nevertheless neglect contributions to the secondary-order convective drift of liquid in the film from these capillary waves since their linear displacement amplitude—typically subnanometer to nanometer in magnitude under the low-input-power conditions in which we observe the film spreading dynamics—are comparable to the displacement amplitude of the SW we had earlier neglected. The transverse and longitudinal SW components given by Eq. (3) determine the magnitude of the leading-order velocity field $f_{-1} = 1/\eta$ and the next order correction $f_0 = 1$. Equating $\mathcal{O}(1/\eta)$ terms then specifies the leading-order

stream-function equation and boundary conditions:

$$\partial_y^4 \psi_{-1}/2 = \partial_t\left(\partial_y^2 \psi_{-1}\right), \tag{7}$$

$$\begin{pmatrix} u_{x,-1} \\ u_{y,-1} \end{pmatrix}_{y=0} = \begin{bmatrix} 0 \\ e^{i(t-x+\varphi)-\alpha x} \end{bmatrix}, \tag{8}$$

$$\begin{pmatrix} \partial_y u_{x,-1} \\ \partial_y u_{y,-1} \end{pmatrix}_{y=h} = \begin{bmatrix} 0 \\ 0 + \mathcal{O}(\eta^2 \mathtt{Ca}^{-1}) \end{bmatrix}. \tag{9}$$

Further equating $\mathcal{O}(0)$ terms gives the next order correction:

$$\partial_y^4 \psi_0/2 = \partial_t\left(\partial_y^2 \psi_0\right), \tag{10}$$

$$\begin{pmatrix} u_{x,0} \\ u_{y,0} \end{pmatrix}_{y=0} = \begin{bmatrix} \chi e^{i(t-x)-\alpha x} \\ 0 \end{bmatrix}, \tag{11}$$

$$\begin{pmatrix} \partial_y u_{x,0} \\ \partial_y u_{y,0} \end{pmatrix}_{y=h} = \begin{bmatrix} 0 \\ 0 + \mathcal{O}(\eta \mathtt{Ca}^{-1}) \end{bmatrix}. \tag{12}$$

It then follows that Eqs. (7)–(9) are satisfied by a unidirectional periodic flow field,

$$\psi_{-1} = \frac{1}{i+\alpha} e^{i(t-x+\varphi)-\alpha x}. \tag{13}$$

Should the film be sufficiently thick, surpassing that of the boundary layer thickness, such that acoustic waves of wavelength $k_l^{*^{-1}}$ generated due to leakage of the SW energy from the substrate can be sustained, this flow field then describes the initial propagation of such waves through the liquid, while still in proximity to the solid substrate. Further, Eqs. (10)–(12) are satisfied by the viscous-dominant periodic vortical flow field,

$$\begin{aligned} \psi_0 = \chi \left(-\frac{1}{4} + \frac{i}{4}\right) \sinh^{-2}\left[\left(\frac{1}{2} + \frac{i}{2}\right) h\right] e^{i(t-x)-\alpha x} \\ \times \{-\sinh\left[(1+i)(y-h)\right] - \sinh\left[(1+i)h\right] \\ + (1+i)y\}. \end{aligned} \tag{14}$$

As noted previously [42], Eq. (14) satisfies only the $\mathcal{O}(1)$ longitudinal velocity of the solid surface and is independent of the $\mathcal{O}(1/\eta)$ transverse motion. Periodic flow to this order may thus be represented as a superposition of the unidirectional and vortical flow fields given by Eqs. (13) and (14), respectively, regardless of their magnitude. This was also hinted in a recent generalized study of vibration-induced flow [47], in which a similar assertion was made by decomposing the flow field into its potential and solenoidal components.

We now show that the next order correction to Eqs. (13) and (14), of magnitude $f_1 \equiv \epsilon/\eta$ and emerging from weak convective interactions between the two above-mentioned leading flow fields, comprises a steady component that dominates over long times. Following a procedure employed earlier [29,34,37,38,42], we decouple the velocity field into its transient and quasisteady components by time averaging the flow field over the fast time scale $\omega^{*^{-1}}$; physically, this is equivalent to the linear periodic component of the flow, which alternates (together with its corresponding harmonics) $\omega^*/2\pi$ times every second, naturally vanishing at the much slower hydrodynamic time scales over which the flow is observed.

Equating the $f_1 \equiv \epsilon/\eta$ magnitude terms, while using a procedure in which we simplify the normal stress condition with the use of the full Navier-Stokes equation [45,46,53], we convert the condition for $\partial_y\langle u_{y,1}\rangle \equiv -\partial_{yx}\langle \psi_1\rangle$ to an equivalent condition for $\partial_{yy}\langle u_{x,1}\rangle \equiv \partial_{yyy}\langle \psi_1\rangle$ that does not involve a derivative of the stream function ψ with respect to x. After time averaging, the quasisteady nonvanishing components of the stream-function equation and boundary conditions can be written as:

$$\partial_y^4\langle \psi_1\rangle/2 = -\left\langle \partial_x \overline{\psi}_{-1} \partial_y^3 \overline{\psi}_0 \right\rangle, \tag{15}$$

$$\begin{pmatrix} \langle u_{x,1}\rangle \\ \langle u_{y,1}\rangle \end{pmatrix}_{y=0} = \begin{pmatrix} 0 \\ 0 \end{pmatrix}, \tag{16}$$

$$\begin{pmatrix} \partial_y\langle u_{x,1}\rangle \\ \partial_{yy}\langle u_{x,1}\rangle \end{pmatrix}_{y=h} = \begin{bmatrix} 0 \\ -(\eta^4/\epsilon \mathtt{Ca})(\partial_{xxx} h + \partial_x p_r - \partial_x \Pi) \end{bmatrix}, \tag{17}$$

where $\overline{\zeta}$ and $\langle\zeta\rangle$ above refer to the real component of the arbitrary function ζ and its time average, i.e., $\langle\zeta\rangle \equiv (1/2\pi)\int_0^{2\pi} \zeta\, dt$. Equations (15)–(17) are satisfied by a long analytical solution for the stream function that we omit here given that it has no particular significance in the present analysis other than to note that the leading-order nonvanishing flow field at long times assumes the magnitude $f_1 = \epsilon/\eta$ and therefore gives rise to the following expression that specifies the nondimensional, nonvanishing, leading-order volume flux in the film, occurring between the streamlines representing the film-substrate and free interfaces:

$$Q = \frac{\epsilon}{\eta}\chi e^{-2\alpha x} f(h(x);\varphi) + \frac{\eta^3}{3\mathtt{Ca}} h^3 \left(\partial_{xxx} h + \partial_x p_r - \partial_x \Pi\right), \tag{18}$$

wherein

$$\begin{aligned} f(h(x);\varphi) \equiv \frac{1}{2(\cos h - \cosh h)^2}\{\sin\varphi(\cos h - \cosh h)^2 \\ + h(\cos h - \cosh h)[\sin h(\sin\varphi + \cos\varphi) \\ + \sinh h(\sin\varphi - \cos\varphi)] + h^2(\sin\varphi \sin h \sinh h \\ - \cos\varphi \cos h \cosh h + \cos\varphi)\}. \end{aligned} \tag{19}$$

The first term on the right-hand side of Eq. (18) quantifies convective contributions to the volume flux from the steady component of the SW-induced flow (i.e., the convective drift) and the second term incorporates contributions from capillary forces, the acoustic radiation pressure, and the disjoining pressure invoked by intermolecular forces such as van der Waals and electrical double layer forces.

The volume flux in Eq. (18) then can be employed to derive the requisite relationship that describes the dynamics of the liquid film under high-frequency SW excitation. Given that the spreading occurs on a hydrodynamic time scale, which is significantly longer than that associated with the period of forcing $\omega^{*^{-1}}$, a choice of two time scales is available: a capillary time scale, associated with the rate at which the spreading at the contact line occurs, and a convective time scale, associated with convective spreading of the film that is invoked by the volumetric drift in Eq. (18). Given that convective spreading

is of interest and capillary forces are weak, as will be shown subsequently, we choose to rescale the time variable with the convective time scale, i.e.,

$$t^* \to \frac{1}{\chi}\frac{\eta}{\epsilon}\frac{k^{*^{-1}}}{U^*}t, \tag{20}$$

in place of the scaling presented earlier in Eq. (2), while retaining all other transformations for the rest of the variables. Together with the scaling in Eq. (2), the dimensionless kinematic condition [46]

$$\partial_t h + \frac{1}{\chi}\frac{\eta}{\epsilon}(u_x\partial_x h - u_y) = 0 \quad \text{at } y = h, \tag{21}$$

subject to continuity

$$\partial_x u_x + \partial_y u_y = 0 \tag{22}$$

and the homogeneous boundary conditions at the liquid-substrate interface in Eq. (16) then lead to the integral mass conservation relationship:

$$\partial_t h + \frac{1}{\chi}\frac{\eta}{\epsilon}\partial_x Q = 0, \tag{23}$$

which, together with Eqs. (18) and (19), give the following relationship that governs the spatiotemporal evolution of the film as it spreads:

$$\partial_t h + \partial_x[e^{-2\alpha x} f(h(x);\varphi)] + \frac{2\Lambda}{3\chi}\partial_x[h^3(\partial_{xxx}h + \partial_x p_r - \partial_x \Pi)] = 0, \tag{24}$$

in which $\Lambda \equiv \eta^2 \mathrm{We}^{-1} = 2k^{*^3}\gamma^*\mu^*/\rho^{*^2}U^{*^2}\omega^*$, with $\mathrm{We} \equiv \rho^* U^{*^2} k^{*^{-1}}/\gamma^*$ being the Weber number that describes contributions to the film dynamics from both the SW-induced convective drift and capillary forces, and $\eta \equiv (\beta^{*^{-1}}/k^{*^{-1}})$. In dimensional terms, Eq. (24) takes the form

$$\partial_t^* h^* + \frac{\chi U^*}{(2\omega^*\mu^*/\rho^*)^{1/2}}\partial_x^*\{e^{-2\alpha^* x^*} f^*[(h^*(x^*)/\beta^{*^{-1}});\varphi]\} + \frac{1}{3\mu^*}\partial_x^*[h^{*^3}(\gamma^*\partial_{x^*x^*x^*}h^* + \partial_x^* p_r^* - \partial_x^*\Pi^*)] = 0, \tag{25}$$

wherein $f^*[(h^*(x^*)/\beta^{*^{-1}});\varphi]$ has units of a volume flux.

Equations (24) and (25) therefore constitute a generalized relationship that describes the different contributions to the high-frequency vibration driven film spreading dynamics, whose transient nature is captured by the first term to the left of the equation. The second term on the left captures SW contributions to the film dynamics through the convective drift flow it invokes; we note that the convective time scale in Eq. (20) renders this term of order unity in dimensional Eq. (24). The last term on the left side of Eq. (24), on the other hand, captures contributions from capillary, acoustic radiation pressure, and intermolecular forces and possesses an order of magnitude that corresponds to that of the dimensionless group Λ. We thus observe that this last term diminishes in magnitude when $\beta^{*^{-1}}$ decreases, resulting in an increase in the relative contribution of the SW-induced convective drift to the film dynamics (given by the second term), consistent with that discussed in Sec. I.

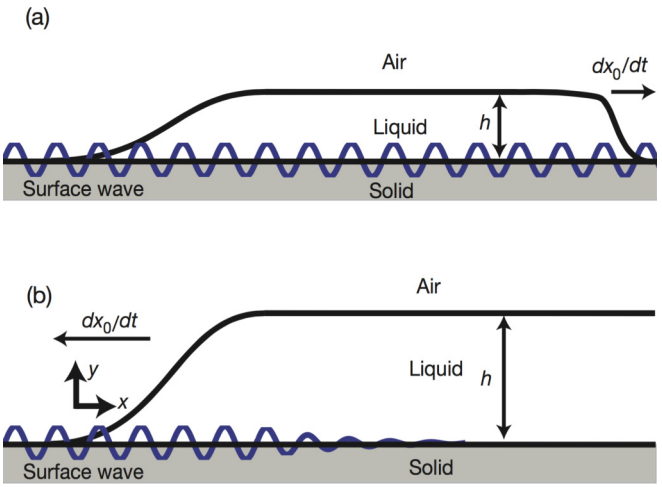

FIG. 3. (Color online) Schematic illustrations of (a) a thin film ($h^* \lesssim \beta^{*^{-1}} \ll k_l^{*^{-1}}$) and (b) a thick film ($h^* \lesssim k_l^{*^{-1}}$), indicating where the SW penetrates the liquid and is attenuated. dx_0/dt denotes the Eulerian film spreading velocity at the film's leading edge. Note that the attenuation of the SAW is negligible for the case of the thin film.

III. DYNAMICS OF THIN FILMS

We now proceed to apply the generalized film spreading relationship given by Eq. (24) to thin liquid films [Fig. 3(a)]: films with thicknesses h that are small compared to the wavelength of the compressional acoustic waves that are generated in the liquid due to leakage of the energy from the SW propagating in the solid, i.e., in dimensional terms $h^* \lesssim \beta^{*^{-1}} \ll k_l^{*^{-1}}$, such that effects due to the acoustic radiation pressure and Eckart streaming—phenomena that are a direct consequence of the generation of acoustic waves in the liquid—are weak and can therefore be ignored. The acoustic waves that leak into the liquid possess similar frequency to that of the SW, although due to the (usually) lower sound speed in the liquid, they typically possess smaller wavelengths compared to that of the SW according to the ratio of the speed of sound in the liquid and the solid. As an example, acoustic waves generated in the half space of water with a sound speed of 1500 m/s due to energy leakage from a 20-MHz SAW with wavelength $2\pi k^{*^{-1}} = 200\ \mu$m propagating along a lithium niobate piezoelectric substrate with a sound speed of approximately 4000 m/s possess a wavelength $2\pi k_l^{*^{-1}} \approx (2\pi k^{*^{-1}}) \times 1500/4000 = 75\ \mu$m.

In this case where the film is too thin to sustain longitudinal bulk acoustic waves within it, the attenuation of the SW itself can also be ignored to leading order. This is because the leakage of SW energy in the form of such bulk acoustic waves now occurs effectively into the air phase above the thin film. For example, the attenuation length for Rayleigh SAWs $\alpha^{*^{-1}} \approx 2\pi\rho_s^* k^{*^{-2}}/\rho_f^* k_l^{*^{-1}}$ [54], in which ρ_s^* is the density of the solid substrate and ρ_f^* the density of the fluid phase the acoustic waves propagate within, suggests that $\alpha^{*^{-1}} \approx 5000$ mm for liquid films that are too thin to sustain bulk acoustic waves—much longer than the length of the substrate itself, which is typically only several millimeters. By comparison, the SW attenuation length $\alpha^{*^{-1}} \approx 1$ mm is much shorter for films with

sufficient thickness to support the propagation of the bulk acoustic waves into them (i.e., $h^* \gg k_l^{*^{-1}}$) and is no longer negligible over the length of the substrate. For SWs in the form of propagating bulk waves, the attenuation length is even longer given the distribution of its mechanical energy throughout the solid substrate. Whichever the case, given that the SW attenuation length scale under thin films is thus much larger than the substrate length itself, it is therefore not unreasonable to impose $\alpha \to 0$ to leading order and to neglect effects due to both the acoustic radiation pressure, i.e., $p_r \approx 0$, and Eckart streaming.

To further simplify the analysis, we expand the volume flux in h:

$$Q = \frac{\chi\epsilon}{\eta}\left[\frac{\cos\varphi}{4}h^2 - \frac{\sin\varphi}{72}h^4 + \mathcal{O}(h^6)\right] + \frac{\eta^3}{3\mathtt{Ca}}h^3\left(\partial_{xxx}h - \partial_x\Pi\right). \tag{26}$$

Here we examine a common case in which the film is excited by SWs in the form of a Rayleigh SAW [5,6] with phase difference $\varphi = 3\pi/2$ (given its retrograde elliptical motion [42]) such that Eq. (26) becomes

$$Q \approx \frac{\chi\epsilon}{\eta}\left[\frac{h^4}{72} + \mathcal{O}\left(h^8\right)\right] + \frac{\eta^3}{3\mathtt{Ca}}h^3\left(\partial_{xxx}h - \partial_x\Pi\right). \tag{27}$$

The leading equation governing the dynamic spreading of the thin film in Eq. (24) then reads

$$\partial_t h + \frac{1}{18}h^3\partial_x h + \frac{2}{3\chi}\Lambda[3h^2\partial_x h\left(\partial_{xxx}h - \partial_x\Pi\right) + h^3\left(\partial_{xxxx}h - \partial_{xx}\Pi\right)] \approx 0. \tag{28}$$

Redimensionalizing Eq. (28) and assuming that the disjoining pressure of the highly wetting silicone oil film is dominated by repulsive van der Waals forces, approximated in dimensional terms for the liquid film geometry by $\Pi^* \equiv A^*/6\pi h^{*3}$, we recover the film spreading equation obtained previously for thin films [8]:

$$\partial_{t^*}h^* + \frac{\chi U^{*^2}}{18\omega^*\beta^{*^{-1}}}\left(\frac{h^*}{\beta^{*^{-1}}}\right)^3\partial_{x^*}h^* + \frac{\gamma^*}{3\mu^*}\partial_{x^*}\left\{h^{*3}\left[\partial_{x^*x^*x^*}h^* + \left(\frac{\mathtt{A}^*}{2\pi\gamma^*}\right)\frac{1}{h^{*4}}\partial_{x^*}h^*\right]\right\} \approx 0. \tag{29}$$

Considering earlier work on inertial film spreading [45], it is clear that a positive convective component [second term on the left-hand side of Eq. (28)] drives the film to spread *along* the drift, which for Rayleigh SAW is *along* the SAW propagation path.

In the derivation of Eq. (29) we have assumed $h^* \approx \beta^{*^{-1}}$, which typically ranges between 10^2 nm and 1 μm for the high-frequency range considered here, such that the convective drift is the underlying driving mechanism for the film spreading. It will be shown later in Sec. IV C that this drift also influences the spreading dynamics for thicker films $h^* \gg \beta^{*^{-1}}$ until the film becomes sufficiently thick to the point at which Eckart streaming, which was not accounted for in Eq. (28), becomes dominant.

In any case, two further characteristic length scales associated with the spreading film dynamics become apparent in Eq. (29): an acoustic capillary length scale $h^*/\beta^{*^{-1}} \approx (\gamma^*\omega^*\beta^{*^{-1}}/\mu^*\chi U^{*^2})^{1/3}$, which arises from a comparison between the kinematic wave velocity $(\chi U^{*^2}/\omega^*\beta^{*^{-1}})(h^*/\beta^{*^{-1}})^3$ in the second term in Eq. (29) and the capillary spreading velocity γ^*/μ^* in the third term of Eq. (29), and a capillary molecular length scale $(\mathtt{A}^*/2\pi\gamma^*)^{1/2}$ in the third term of Eq. (29). In the former, both capillary and convective stresses balance when $h^*/\beta^{*^{-1}} \approx 1$. In other words, we expect convective stresses to be dominant and hence to generate drift in thicker films, whereas capillary stresses are dominant in thinner films. For the latter, we note that the capillary molecular length scale is typically on the order of 1–10 nm (for $\mathtt{A}^* \approx 10^{-19}$ J), which is significantly smaller than the acoustic capillary length scale such that the effects of the SW excitation diminish at these thicknesses close to the contact line and the spreading film dynamics is governed by the usual balance between capillary and disjoining pressure.

For completeness, we highlight the insight that can be gleaned from the singular limit of Eq. (29), wherein capillary terms are small. Rescaling the time variable by $t^* \to (18\omega^*\beta^{*^{-1}}k^{*^{-1}}/\chi U^{*^2})t$, we arrive at the kinematic wave equation

$$\partial_t h + h^3\partial_x h \approx 0 \tag{30}$$

by accounting for integral conservation of mass, which, under constant density, can be written as

$$\int_{x=0}^{x_0(t)} h\,dx = \text{const}, \tag{31}$$

where $x = x_0(t)$ is the position of the front of the spreading film. A similarity solution for the above equations was then obtained by introducing the similarity transformation:

$$\xi \equiv x/t^a, \quad H \equiv h/t^b, \quad t = \tau, \tag{32}$$

which, upon substitution, renders Eqs. (30) and (31) time independent, i.e., $\partial_\tau H = 0$, when $3b - a + 1 = 0$ and $a = -b$. It then follows that $a = 1/4$ and $b = -1/4$ such that at long times the leading edge of the film spreads as

$$x_0 \sim t^{1/4}, \tag{33}$$

while the film decreases in height as

$$h(x) \sim t^{-1/4}, \tag{34}$$

eventually approaching a singularity as the rear of the film catches up with its advancing front. This then results in the steepening of the slope near the advancing front where the influence of capillary and intermolecular forces, though assumed insignificant to begin with, becomes sufficiently strong to overcome the assumed initial dominance of the convective term assumed in Eq. (30). This quantitative picture, and, in particular, the similarity scalings given by Eqs. (33) and (34), are remarkably consistent with the experimental data obtained for thin silicone oil films spreading under the influence of MHz-order Rayleigh SAWs [8].

IV. DYNAMICS OF THICK FILMS

We now return to the generalized film spreading equation we have derived in Eq. (24) to examine films of larger thicknesses, i.e., films with sufficient thicknesses ($h^* \gtrsim k_l^{*^{-1}} \gg \beta^{*^{-1}}$) to support the leakage of the SW energy into the fluid in the form of acoustic waves. To do so, we, however, first discuss how the acoustic radiation pressure potentially influences the stability of the film.

A. Acoustic radiation pressure

Due to the large difference in the acoustic impedance (density multiplied by the bulk sound speed) across the free surface of the liquid, the transfer of momentum associated with the generation of acoustic waves in the liquid upon leakage of the SW energy into the liquid from the substrate produces a net steady force on the free surface over long times ($t^* \gg 1/\omega^*$). This is known as the acoustic radiation pressure [43,48,49,55,56] and takes the generalized form

$$p_r^* = (p^*\mathbf{I}\cdot\mathbf{n})\cdot\mathbf{n} + (\langle\rho^*\mathbf{u}^*\mathbf{u}^*\rangle\cdot\mathbf{n})\cdot\mathbf{n}, \tag{35}$$

where $\mathbf{I}$ and $\mathbf{n}$ are the identity tensor and the unit outward normal vector to the free surface, respectively. In particular, we examine acoustic radiation pressure effects along the nearly flat portion of the free surface of the film away from its advancing front in the vicinity of the contact line. These nearly flat free surfaces serve as near-ideal reflectors (as a consequence of the large jump in the acoustic impedance across the free surface) of the acoustic waves that form in the liquid due to leakage off the SW energy and give rise to acoustic resonances and antiresonances within the film, thus leading to appreciable acoustic radiation pressure effects at specific film thicknesses.

More specifically, the acoustic waves propagating in a liquid can be described predominantly by a potential flow field generated by the normal component of the SW velocity u_y^*, whose local form, we assume, for simplicity, resembles the completely in-phase vertical substrate motion of a pistonlike acoustic wave transducer—reasonable given $h^*/k^{*^{-1}} \sim 1$. It then follows that the parallel acoustic waves generated from such pistonlike motion of the substrate produces an acoustic radiation pressure at the free surface, which, in dimensionless form, reads [5]

$$p_r = \frac{\mathrm{We}_a e^{-2\alpha x}\left[1 + O\left(hk_l\right)\right]}{\cos^2\left[\left(k_l/\beta\right)h\right]\sin^2\left[\left(k_l/\beta\right)h\right]}, \tag{36}$$

where $\mathrm{We}_a \equiv (1 + B/2A)\rho_a^* U^{*^2} k^{*-1}/8\eta\gamma^*$ is an acoustic Weber number that describes the relative magnitudes of the acoustic radiation and capillary pressures acting at the free surface, B and A are the Fox and Wallace coefficients [49], and ρ_a^* is the density of the air phase above the liquid film. It then can be seen from Fig. 4 that p_r decays to negligible values in the vicinity of each of its minima at $h^*/2\pi k_l^{*-1}\beta^* = (1 + 2i)/8$ ($i = 0,1,2,\ldots$) and becomes singular at $h^*/2\pi k_l^{*-1}\beta^* \to 2i/8$ ($i = 0,1,2,\ldots$), suggesting that the film, being nearly flat, is quantized to specific thickness values, consistent with previous experimental observations [5,6,8]. In particular, low-surface-energy oil films were found to spread with a characteristic film thickness corresponding to $i = 1$ [8] and $i = 3$ [6] while high-surface-energy water films were found to form a cascading series of flat films with thicknesses corresponding to $i \geqslant 7$ [5].

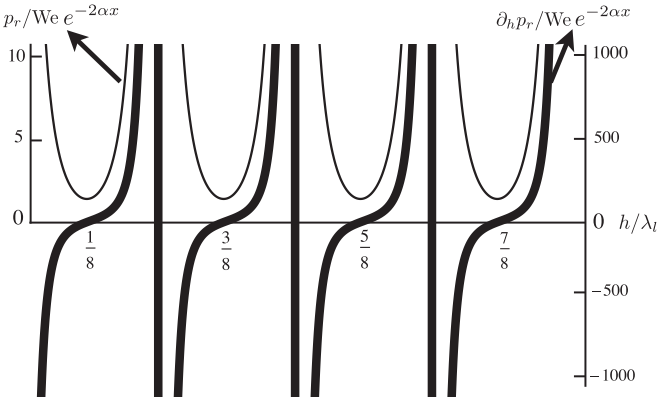

FIG. 4. Dimensionless acoustic radiation pressure and its gradient as a function of the scaled film thickness.

We note that the above is not applicable for the thin films with dimensional thickness $h^* \ll k_l^{*^{-1}}$ considered earlier in Sec. III since Eq. (36) was derived under the dimensional assumption that $h^* \approx k_l^{*^{-1}}$ such that the pressure singularity appearing in Eq. (36) and illustrated in Fig. 4 for the limit $h \to 0$ is not valid; in the present analysis, the acoustic pressure singularities occur due to resonances of the acoustic wave generated within the film as a consequence of leakage of the SW energy into the liquid, which, as discussed earlier, were not supported in sufficiently thin films with dimensional thicknesses corresponding to $h^* \ll k_l^{*^{-1}}$. More specifically, p_r^* is linearly proportional to the average excess acoustic energy in the film, i.e., $p_r^* \propto \langle E^*\rangle$, where along the path of the acoustic waves emitted by the SW [49],

$$E^* = \frac{\omega^*}{2k_l^*}\frac{\rho^{*^L} - \rho^*}{\rho^*} + \frac{\rho^* u_y^{*^{L2}}}{2}; \tag{37}$$

the right-hand side of the equation describes the Lagrangian excess potential and kinematic energies with respect to the normal SW velocity, arising from the deviation of the Lagrangian density and normal velocity fields, ρ^{*^L} and $u_y^{*^L} = u_y^* - e^{i(t^*-x^*+\varphi)-\alpha^* x^*}/\eta$, from their equilibrium values, ρ^* and $u_y^* = 0$, respectively. For sufficiently thin films of thickness $h^* \lesssim \beta^{*^{-1}} \ll k_l^{*^{-1}}$ that do not permit the generation of acoustic waves in the liquid, the flow in the film is strictly the unidirectional flow field in Eq. (13), which, together with $u_y^{*^L} = 0$ and $\rho^{*^L} = \rho^*$ that causes the excess energy in the film in Eq. (37) to vanish, gives

$$p_r \approx 0. \tag{38}$$

Next we highlight the insight gained from an examination of the film stability under the influence of the spatially periodic acoustic radiation pressure given by Eq. (36) as well as the film spreading dynamics when they are exposed to such acoustic radiation pressure.

B. Stability of the film thickness

Recalling an earlier result [8], we subject the nearly flat film of thickness h_0, i.e., the steady "base state" component, to a small perturbation along the longitudinal axis $\delta g(x,t) \equiv \delta C e^{inx+\sigma t}$, where $\delta \ll 1$, C is an arbitrary constant, n is the wave number of a film thickening mode, and σ is the rate of growth of the film's dynamic response to small interferences in its thickness h_0:

$$h(x,t) = h_0 + \delta g(x,t). \tag{39}$$

Expanding Eq. (24) and retaining the leading-order $\mathcal{O}(\delta)$ linear terms then gives

$$\frac{\sigma}{2\Lambda/3\chi} = (\partial_h p_r|_{h=h_0})n^2 - n^4 + \cdots, \tag{40}$$

in which the remaining expression in the equation above consists of the convective terms in Eq. (24) that comprise oscillatory complex components which do not affect the film's stability. From Eq. (40), it appears that capillary forces act to stabilize the film, whereas the acoustic radiation pressure may act to destabilize it. Further, it is apparent that a negative radiation pressure slope, i.e., $\partial_h p_r|_{h=h_0} < 0$, renders σ negative, resulting in a stable film; a positive radiation pressure slope, i.e., $\partial_h p_r|_{h=h_0} > 0$, on the other hand, may render σ positive for certain values in the radiation pressure slope and thus produce an unstable film. We thus highlight the linear rate growth coefficient of the film thickness σ for $\partial_h p_r|_{h=h_0} > 0$ by transforming Eq. (40) to

$$\frac{\sigma}{2\Lambda(\partial_h p_r|_{h=h_0})^2/3\chi} = \left(\frac{n}{\sqrt{\partial_h p_r|_{h=h_0}}}\right)^2 - \left(\frac{n}{\sqrt{\partial_h p_r|_{h=h_0}}}\right)^4 + \cdots, \tag{41}$$

which is illustrated in Fig. 5. It then becomes apparent that for $\partial_h p_r|_{h=h_0} > 0$, the film becomes unstable ($\sigma > 0$) under sufficiently small disturbance wave numbers ($n/\sqrt{\partial_h p_r|_{h=h_0}} < 1$), i.e., for sufficiently large wavelength disturbances along the free surface of the film.

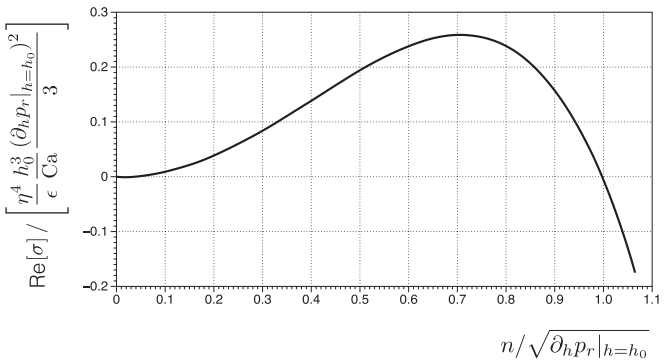

FIG. 5. Variation in the linear film thickness growth rate σ with the disturbance wave number n for positive values in the acoustic radiation pressure slope ($\partial_h p_r|_{h=h_0} > 0$), which renders the film thickness unstable ($\sigma > 0$) under sufficiently small disturbance wave numbers ($n/\sqrt{\partial_h p_r|_{h=h_0}} < 1$); we exclude complex contributions to σ.

Should the film thickness h be sufficiently small, i.e., $h^* \lesssim k_l^{*^{-1}}/8$, then $\partial_h p_r|_{h=h_0} < 0$ and the film is stable; we note that the film remains stable even with further decreases in the film thickness such that $h^* \lesssim \beta^{*^{-1}} \ll k_l^{*^{-1}}$, wherein the acoustic radiation pressure becomes negligible [see Eq. (38)]. In contrast, should the film thickness be sufficiently large to support the nonmonotonic thickness variation in p_r given by Eq. (36), we find that σ may either be positive (unstable) or negative (stable) depending on the rate at which the acoustic radiation pressure varies with the film thickness $\partial_h p_r|_{h=h_0}$. If $\partial_h p_r|_{h=h_0} < 0$, the acoustic radiation pressure forces the free surface upwards and hence causes the film to thicken, which, in turn, leads to a decrease in the acoustic radiation pressure, thus producing a stable film thickness. On the other hand, if $\partial_h p_r|_{h=h_0} > 0$, film thickening further increases the acoustic radiation pressure that, in turn, causes further growth in the film's thickness, therefore resulting in an unstable film. This can be seen in Fig. 5 where the real component of σ is plotted against n for $\partial_h p_r|_{h=h_0} > 0$, from which we note that the film is unstable to longwave disturbances whose dimensionless wave number is smaller than the imposed square root of the dimensionless acoustic radiation pressure gradient, i.e., $n < \sqrt{\partial_h p_r}$, with $n/\sqrt{\partial_h p_r|_{h=h_0}} = 2/\sqrt{2}$ being the "most dangerous" disturbance mode at which the instability growth rate is at its maximum value. We therefore conclude that sufficiently thin films, such as those discussed in Sec. III where $h^* \lesssim k_l^{*^{-1}}/8$, are stable irrespective of their thicknesses whereas thicker films for which $h^* \gtrsim k_l^{*^{-1}} \gg \beta^{*^{-1}}$ will generally assume stable thickness values that satisfy $\partial_h p_r|_{h=h_0} \leqslant 0$, translating to the dimensional thickness range

$$\frac{2i}{8} < \frac{h^*}{2\pi k_l^{*^{-1}}} < \frac{1+2i}{8} \quad (i = 1,2,\ldots). \tag{42}$$

C. Spreading dynamics

We now turn our attention to the spreading dynamics of thick films, such that $h^* \lesssim k_l^{*^{-1}}$, where contributions to spreading due to the acoustic radiation pressure and SW attenuation become appreciable. Such thick films are found to spread in the opposite direction to that of the Rayleigh SAW propagation [6] and thus the drift the SAW invokes in the film, opposing the spreading direction of the thin films considered in Sec. III. Here, in particular, we show the validity of the generalized film equation in Eq. (24) for describing the spreading dynamics of these films by showing that the expression for the spreading velocity of thick films derived earlier [6,8] can be recovered from our unified theory, subject to an $\mathcal{O}(1)$ correction due to the explicit inclusion of the normal stress condition at the free surface of the film in the present analysis.

Under high-frequency SW excitation, films with thicknesses comparable to the acoustic wavelength in the liquid, i.e., $h^* \gtrsim k_l^{*^{-1}} \gg \beta^{*^{-1}}$ (typically 10–10^2 μm for common liquids and for the system parameters specified in Sec. II), result in appreciable SW energy leakage from the substrate and into the predominantly flat liquid film [Fig. 3(b)] in the form of acoustic waves; as a consequence, there exists appreciable attenuation of the SW and acoustic radiation pressure is imparted at the free surface of the film. The interplay between capillary forces and

the acoustic radiation pressure then imposes the stable periodic film thickness constraint given by Eq. (42), at least along the flat film region away from the *curved* capillary ridge region at the advancing film front next to the three-phase contact line. These films are nevertheless too thin for Eckart streaming effects to become appreciable (which requires $h^* \gg k_l^{*^{-1}}$) so the spreading film dynamics is governed predominantly by capillary forces, the SW-induced acoustic radiation pressure, and convective drift.

In the following, we simplify Eq. (24) using assumptions that are appropriate for the thick film geometry in order to attain a leading-order equation that can be solved analytically. Away from the region of the curved film meniscus, the film thickness h approaches a stable nominal value h_0—considered large with respect to the viscous penetration length since $\beta^{*^{-1}} \ll k_l^{*^{-1}}$ (i.e., in dimensionless terms, $h_0 \gg 1$) [33,34,47]—specified by a dominant balance between the capillary and acoustic radiation pressures in Eq. (42), i.e., $h \approx h_0$ to leading order. In addition, since the thickness of the film away from the meniscus is much greater than the viscous penetration length, i.e., $h_0^* \gg \beta^{*^{-1}}$ (see Sec. III), it is possible to simplify the volume flux by taking Q in the limit $h_0^*/\beta^{*^{-1}} \gg 1$ (or, in dimensionless terms, $h_0 \gg 1$). Further, since $\Lambda \approx 10^{-1}$ in Eq. (24) for the characteristic range of experimental parameters specified in Sec. II, we ignore, to first approximation, contributions that appear from the meniscus region of the advancing film. The generalized film equation in Eq. (24) then simplifies to

$$\partial_t h \approx -\partial_x \left[\frac{\chi e^{-2\alpha(x-x_0)}}{2} (\cos\varphi - \sin\varphi)\, h \right]; \qquad (43)$$

$x = x_0$ is taken to be the position of the advancing film front where the SW first encounters the liquid film and continues to propagate under the film but with appreciable attenuation.

We transform Eq. (43) into Lagrangian coordinates with an origin attached to the Eulerian coordinate $x = x_0(t)$, where the film becomes flat ($h \approx h_0$) and where SAW attenuation commences, using the Galilean transformation $x \to x - x_0$ and $dh/dt = \partial_t h + (dx_0/dt)\partial_x h$, assuming dx_0/dt is a weak function of time; dh/dt is the material derivative of the film thickness. Taking the advancing front to be stationary in the Lagrangian frame of view ($dx_0/dt \approx 0$) then renders

$$\partial_x h \frac{dx_0}{dt} \approx \partial_x \left[\frac{\chi e^{-2\alpha x}}{2} (\cos\varphi - \sin\varphi)\, h \right]. \qquad (44)$$

Given $\alpha^{*^{-1}} \approx 1$ mm [54] in dimensional terms for the range of experimental parameters employed in Sec. II, it is reasonable to assume that the SW attenuation length is short with respect to the length of the film but long with respect to the length scale of the capillary ridge at the advancing film front. Consequently, the attenuation of the SW along the substrate beneath the meniscus at the film front can be considered negligible. Since the advancing front of the meniscus is at $x = 0$, we assume $h/h_0 \to 0$ at $x \to -\infty$ and $h/h_0 \approx 1$ for $x > 0$. We then integrate Eq. (44) from $x \to -\infty$ to $x \to \infty$, where we assume as before that dx_0/dt is constant. As we ignore contributions from the meniscus, the limits of the integral on the right-hand side of the equation are equivalent to an integration from $x \to 0$ to $x \to \infty$, giving

$$\frac{dx_0}{dt} \approx -\frac{\chi}{2} (\cos\varphi - \sin\varphi)\,, \qquad (45)$$

or, in a dimensional form,

$$\frac{dx_0^*}{dt^*} = -\frac{\chi}{2}\frac{\epsilon}{\eta} U^* (\cos\varphi - \sin\varphi)$$
$$= -\frac{\chi}{2}\frac{U^{*^2}}{\omega^* \beta^{*^{-1}}} (\cos\varphi - \sin\varphi). \qquad (46)$$

The relationship above then describes the dynamic spreading of the film's leading edge. For SWs in the form of Rayleigh SAWs ($\varphi = 3\pi/2$), it can then be seen that the film spreads in a direction opposing that of the SW propagation, consistent with that alluded to above. In contrast, other forms of SW excitation, such as Sezawa SAWs where $\varphi = \pi/2$, will drive film spreading along the direction of the wave propagation in the solid. In both cases, however, the film spreads in the direction opposite to that of the SW-induced drift. This counterintuitive effect wherein the film spreads in opposition to the direction of the SW-induced drift, which is not obvious from the governing equations, is due to the constant film thickness constraint imposed by the acoustic radiation pressure, at least away from the meniscus region at the advancing film front; mass conservation then requires the film to spread in the direction opposite to that of the imposed internal volume flux. This can be strongly contrasted with the spreading of most other films via conventional means such as gravity- or Marangoni-driven spreading in which the film continuously increases in thickness near the advancing front due to the imposed internal volume flux and decreases in thickness along the rear to conserve mass, resulting in film spreading along the direction of the film's internal volume flux. This constitutes the mechanics of spreading of thin films in Sec. III where it is clear that a positive convective component [second term on the left of Eq. (28)] drives the film to spread *along* the drift through a pseudo kinematic wave equation when capillary contributions in Eq. (28) are omitted.

It is, however, apparent that we obtain a slightly different 1/2 numerical prefactor in Eqs. (45) and (46) compared to the $1/6 \log 2$ numerical prefactor in earlier work [6,8]. As noted above, this difference arises from the simplifying assumption made in the earlier work that omitted an explicit normal stress balance at the free surface of the film.

V. CONCLUDING REMARKS

In this work, we have derived a generalized model that governs the dynamic spreading behavior of liquid films on substrates under high-frequency (MHz-order) vibration in the form of propagating SWs. In particular, the film spreading dynamics is driven by the invocation of a dominant viscous periodic flow, which supports a weak convective and steady contribution in the form of a confined Reynolds stress that may translate into an effective surface force or an equivalent convective drift near the contact line region. In fact, the role of $\beta^{*^{-1}}$ is prevalent and appears throughout the expressions governing the spreading in various cases, be it in the point surface force that arises due to the coarse-grained Reynolds

stress on the interface in the case of low-surface-energy substrates where the initial contact angles are large [4] or in the velocity of the advancing front in Eq. (46) for thick films on high-surface-energy substrates [6]: The smaller the value of $\beta^{*^{-1}}$ as the excitation frequency is increased, the larger the force or the velocity. Both directionality and phase of the substrate excitation are also found to play an important role, influencing the direction along which the film spreads: Spatially isotropic vibration on the substrate was found to render axisymmetric spreading in all directions, whereas directionally propagating SWs were found to render spreading along a specific direction, influenced by the phase of the SW between its longitudinal and transverse component.

The diversity of thickness scales that a liquid body can assume then yields various scenarios for the spreading film. This is captured through the generalized film spreading relationship given by Eq. (25), which governs the counterintuitively opposing spreading dynamics of thin and thick films that predominantly arise as a consequence of the convective drift generated by the dominant viscous periodic flow, which is a consequence of the direct interaction between the undulating substrate boundary as the SW traverses it and the liquid in the film immediately adjacent to it.

Sufficiently thin films with thicknesses beyond molecular length scales $h^* \approx (A^*/2\pi\gamma^*)^{1/2} \approx 1$–$10$ nm, where capillary and intermolecular forces are dominant, and within the range $h^* \lesssim \beta^{*^{-1}} \approx 0.1$–$1$ μm, are governed by a balance between capillary stresses and the SW-invoked drift in the film. As these thin films are not sufficiently thick to support the propagation of acoustic waves into the liquid due to the leakage of SW energy from the substrate, the acoustic radiation pressure acting on the interface is negligible and hence beyond this thickness, i.e., $h^* \gtrsim \beta^{*^{-1}} \ll k_l^{*^{-1}}$, the convective drift generated by the dominant viscous periodic flow highlighted in Eq. (29) constitutes the primary mechanism that drives the spreading in the same direction of the drift, which, in turn, is along the propagation direction of the SW for the case of Rayleigh SAWs. In the inertial limit, in which the convective drift dominates the film dynamics over capillary effects, the film is observed to spread self-similarly as $t^{1/4}$, consistent with that observed in previous experiments.

Films of larger thicknesses ($h^* \lesssim k_l^{*^{-1}} \approx 10$–$10^3$ μm), on the other hand, permit the leakage of the SW energy from the substrate to produce MHz compressional acoustic waves in the liquid and are therefore influenced by an additional stress mechanism, namely the acoustic radiation pressure, leading to periodically stable and unstable films (or regions within a film), as predicted by the linear stability theory in Eq. (42). Together with the drift flow, they give rise to a volume flux that causes the film to spread with constant velocity according to Eq. (46) in the direction that opposes the drift flow and, in the case of Rayleigh SAWs, in the direction opposite to that of the SW propagation, which is also consistent that observed to date.

ACKNOWLEDGMENTS

O.M. acknowledges funding in support of this work by the CIG FP-7 PEOPLE Programme (Marie Curie Actions) under Project No. 615650. L.Y.Y. gratefully acknowledges support through a Future Fellowship from the Australian Research Council through Grant No. FT130100672.

[1] A. Qi, L. Yeo, and J. Friend, Phys. Fluids **20**, 074103 (2008).
[2] M. Alvarez, J. Friend, and L. Yeo, Langmuir **24**, 10629 (2008).
[3] M. Tan, J. Friend, O. Matar, and L. Yeo, Phys. Fluids **22**, 112112 (2010).
[4] O. Manor, M. Dentry, J. Friend, and L. Yeo, Soft Matter **7**, 7976 (2011).
[5] D. J. Collins, O. Manor, A. Winkler, H. Schmidt, J. R. Friend, and L. Y. Yeo, Phys. Rev. E **86**, 056312 (2012).
[6] A. Rezk, O. Manor, J. Friend, and L. Yeo, Nat. Commun. **3**, 1167 (2012).
[7] J. Blamey, L. Yeo, and J. Friend, Langmuir **29**, 3835 (2013).
[8] A. Rezk, O. Manor, L. Yeo, and J. Friend, Proc. R. Soc. A. **470**, 20130765 (2014).
[9] S. Biwersi, J. Manceau, and F. Bastien, J. Acoust. Soc. Am. **107**, 661 (2000).
[10] J. Scortesse, J. Manceau, and F. Bastien, J. Sound Vib. **254**, 927 (2002).
[11] X. Noblin, A. Buguin, and F. Brochard-Wyart, Eur. Phys. J. E **14**, 395 (2004).
[12] S. Alzuaga, J.-F. Manceau, and F. Bastien, J. Sound Vib. **282**, 151 (2005).
[13] S. Daniel, M. Chaudhury, and P. DeGennes, Langmuir **21**, 4240 (2005).
[14] J. Bennès, S. Alzuaga, P. Chabé, G. Morain, F. Chérioux, J. Manceau, and F. Bastien, Ultrasonics **44**, e497 (2006).
[15] D. Lyubimov, T. Lyubimova, and S. Shklyaev, Phys. Fluids **18**, 012101 (2006).
[16] E. Bormashenko, R. Pogreb, G. Whyman, and M. Erlich, Langmuir **23**, 6501 (2007).
[17] P. Brunet, J. Eggers, and R. D. Deegan, Phys. Rev. Lett. **99**, 144501 (2007).
[18] I. Fayzrakhmanova and A. Straube, Phys. Fluids **21**, 072104 (2009).
[19] P. Brunet, J. Eggers, and R. Deegan, Eur. Phys. J. Spec. Top. **166**, 11 (2009).
[20] M. Strani and F. Sabetta, J. Fluid Mech. **141**, 233 (1984).
[21] E. Wilkes and O. A. Basaran, Phys. Fluids **9**, 1512 (1997).
[22] T. Benjamin and F. Ursell, Proc. R. Soc. Lond. A **225**, 505 (1954).
[23] J. Xu and D. Attinger, Phys. Fluids **19**, 108107 (2007).
[24] X. Noblin, A. Buguin, and F. Brochard-Wyart, Phys. Rev. Lett. **94**, 166102 (2005).
[25] E. B. Dussan V. and R. T.-P. Chow, J. Fluid Mech. **137**, 1 (1983).
[26] L. Hocking, J. Fluid Mech. **179**, 253 (1987).
[27] L. Hocking, J. Fluid Mech. **179**, 267 (1987).
[28] G. Batchelor, *An Introduction to Fluid Dynamics* (Cambridge University Press, Cambridge, 1967).
[29] H. Schlichting, Phys. Z. **33**, 327 (1932).
[30] W. Nyborg, J. Acoust. Soc. Am. **25**, 1 (1952).

[31] M. Longuet-Higgins, Philos. Trans. R. Soc. Lond. **245**, 535 (1953).
[32] J. Holtsmark, I. Johnsen, T. Sikkeland, and S. Skavl, J. Acoust. Soc. Am. **26**, 26 (1954).
[33] N. Riley, Mathematika **12**, 161 (1965).
[34] J. Stuart, J. Fluid Mech. **24**, 673 (1966).
[35] T. W. Secomb, J. Fluid Mech. **88**, 273 (1978).
[36] N. Riley, J. Fluid Mech. **180**, 319 (1986).
[37] N. Riley, Theoret. Comput. Fluid Dynam. **10**, 349 (1998).
[38] N. Riley, Annu. Rev. Fluid Mech. **33**, 43 (2001).
[39] H. Schlichting and K. Gersten, *Boundary-Layer Theory*, 8th ed. (Springer-Verlag, Berlin, 2003).
[40] P. Westervelt, J. Acoust. Soc. Am. **25**, 60 (2004).
[41] C. Wang, J. Fluid Mech. **32**, 55 (2005).
[42] O. Manor, L. Yeo, and J. Friend, J. Fluid Mech. **707**, 482 (2012).
[43] J. Friend and L. Yeo, Rev. Mod. Phys. **83**, 647 (2011).
[44] L. Yeo and J. Friend, Annu. Rev. Fluid Mech. **46**, 379 (2014).
[45] D. Benny, J. Math. Phys. **45**, 150 (1966).
[46] R. Craster and O. Matar, Rev. Mod. Phys. **81**, 1131 (2009).
[47] J. Vanneste and O. Buhler, Proc. R. Soc. Lond. A **467**, 1779 (2011).
[48] L. King, Proc. R. Soc. Lond. A **147**, 212 (1934).
[49] B. Chu and R. Apfel, J. Acoust. Soc. Am. **72**, 1673 (1982).
[50] C. Eckart, Phys. Rev. **73**, 68 (1948).
[51] J. Lighthill, J. Sound Vib. **61**, 391 (1978).
[52] W. Krantz and S. Goren, Ind. Eng. Chem. Fundam. **9**, 107 (1970).
[53] A. Oron, S. Davis, and S. Bankoff, Rev. Mod. Phys. **69**, 931 (1997).
[54] R. M. Arzt, E. Salzmann, and K. Dransfeld, Appl. Phys. Lett. **10**, 165 (1967).
[55] T. Hasegawa, T. Kido, T. Iizuka, and C. Matsuoka, J. Acoust. Soc. Jpn. E **21**, 146 (2000).
[56] F. Borgnis, Rev. Mod. Phys. **25**, 653 (2010).